Research article

Computational analysis of bio-convective eyring-powell nanofluid flow with magneto-hydrodynamic effects over an isothermal cone surface with convective boundary condition

P. Francis [a], P. Sambath [a,**], U. Fernandez-Gamiz [b], S. Noeiaghdam [c,*], S. Dinarvand [d]

[a] Department of Mathematics, SRM Institute of Science and Technology, Kattankulathur, Tamil Nadu 603203, India
[b] Nuclear Engineering and Fluid Mechanics Department, University of the Basque Country UPV/EHU, Nieves Cano 12, 01006 Vitoria-Gasteiz, Spain
[c] Faculty of Applied Mathematics and Programming, South Ural State University, Lenin Prospect 76, Chelyabinsk-35004, Russia
[d] Department of Mechanical Engineering, Central Tehran Branch, Islamic Azad University, Tehran, Iran

ARTICLE INFO

ABSTRACT

Non-Newtonian fluids are essential in situations where heat and mass transfer are involved. Heat and mass transfer processes increase efficiency when nanoparticles ($0.01 \leq \varphi \leq 0.03$) are added to these fluids. The present study implements a computational approach to investigate the behavior of non-Newtonian nanofluids on the surface of an upright cone. Viscous dissipation ($0.3 \leq E_c \leq 0.9$) and magnetohydrodynamics (MHD) ($1 \leq M \leq 3$) are also taken into account. Furthermore, we explore how microorganisms impact the fluid's mass and heat transfer. The physical model's governing equations are transformed into ordinary differential equations (ODEs) using a similarity transformation to make the analysis easier. The ODEs are solved numerically using the Bvp4c solver in MATLAB. The momentum, thermal, concentration, and microbe diffusion profiles are graphically represented in the current research. MHD ($1 \leq M \leq 3$) effects improve the diffusion of microbes, resulting in increased heat and mass transfer rates of 18 % and 19 %, respectively, based on our results. Furthermore, a comparison of our findings with existing literature demonstrates promising agreement.

1. Introduction

In numerous sectors like the chemical-based, nutrition, brewing, and soft drinks industries, as well as the metallurgy and factories, plastics, and textile sectors, conical-shaped items are commonly used. After being used, these cone-shaped things often need to be cooled down quickly so that industrial processes can continue without interruption. Because the industry depends on these cone-shaped parts, they need to cool down quickly. This makes their quick repair very important. For instance, vertical cone mixers are very important for making safe, premium products like medicine, food, and personal hygiene items that are consumed all over the world. Each type of upright cone mixer is made with a different set of industrial goals in mind. It is clear that grinding is more effective when upright cone mixers are used, which causes the surface of the mixer to warm up on the cone. This heating happens because the

* Corresponding author.
** Corresponding author.
E-mail addresses: fp9469@srmist.edu.in (P. Francis), sampathp@srmist.edu.in (P. Sambath), unai.fernandez@ehu.eus (U. Fernandez-Gamiz), noiagdams@susu.ru (S. Noeiaghdam), sae.dinarvand@iauctb.ac.ir, saeed_dinarvand@yahoo.com (S. Dinarvand).

Cp_{nf}, Cp_f **Nomenclature**

b	Chemo-taxis constant
B_0^2	Dimension magnetic parameter
B_1	Biot number
C	Concentration
Cp_{nf}, Cp_f	Specific heat
d	Physical Eyring-Powell fluid parameter
D	Mass diffusion
D_n	Diffusion of microorganisms
f	Dimensionless velocity function
h_f	Convective heat transfer coefficient
J_u	Joule heating parameter
k_1	porosity parameter
K	Dimensionless Eyring-Powell parameter
L_b	Bio-convection Lewis number
M	Dimensionless magnetic parameter
N	Density of microorganisms
N_1	Non-Newtonian fluid parameter
N_r	Buoyancy ration parameter
P_r	Prandtl number
P_e	Bio-convection Peclet number
R_b	Bio-convection Rayleigh number
S_c	Schmidt number
T	Temperature
u, v	Velocity component
W_c	The maximum cell swimming speed
x, y	Coordinate

Greek symbols

α_{nf}	Thermal diffusion of nanofluid
β	Characteristics of the Eyring-Powell fluid
$\beta_T, \beta_C, \beta_N$	The volumetric expansion of thermal, concentration and microorganisms
γ	The average volume of microorganisms
Γ	Dimensionless porosity constant
θ	Dimensionless temperature function
μ_{nf}, μ_f, μ_s	Dynamic viscosity
ν_{nf}, ν_f	Kinematic viscosity
ξ	Dimensionless boundary layer coordinate
$\rho_{nf}, \rho_f, \rho_s$	Density
σ	Bio-convection constant
φ	The volume fraction of nanofluid
φ	Dimensionless concentration function
χ	Dimensionless microorganism's density function
ψ	Stream function
ω	Half angle of the vertical cone

Subscripts

f	State of the base fluid
nf	State of the nanofluid
s	State of the nanoparticle
w	State of the wall
∞	State of the ambient

mixture is mixed quickly and well, which moves heat along the surface of the cone. In the pursuit of effective cooling for these cones, it has been observed that non-Newtonian fluids yield superior results when compared to conventional fluids. In the present scenario, we will concentrate on Eyring-Powell fluid, a type of non-Newtonian fluid. Adding nanofluids ($Cu, Ag, Al_2 O_3 \ \ and \ TiO_2$) has also been shown to improve the effectiveness of heat transfer. By utilizing magnetohydrodynamics (MHD), we suggest solutions for the detrimental effects of microorganisms on heat and mass transfer processes, which are investigated in the current study.

The Non-Newtonian model for heat transfer and its applications have been extensively studied in the literature [1–5]. The influence of Magnetohydrodynamics (MHD) is of paramount importance in the context of heat transfer and finds numerous applications in engineering. Several investigations have examined heat transfer in MHD fluids, particularly in cases involving Newtonian and non-Newtonian fluid flow over varying geometries [6–10]. Ahmed [11] and Peng Xu et al. [12] conducted a study on the convection flow that is naturally occurring on a vertical cone surface, focusing on the implications of improved heat transmission. Several other researchers [13–15] used computational techniques to study the characteristics of Newtonian as well as non-Newtonian fluids in various designs for the purpose of understanding heat exchange. Building upon this prior work, Bapuji Pullepu and Sambath [16] and Hamad [17] explored free convection problems in the presence of nanofluids and discovered that nanofluids enhance both heat and mass transfer. Sami Ullah Khan et al. [18] and Imad Khan et al. [19] studied the behavior of non-Newtonian fluids, specifically Eyring-Powell fluids, in flow over-stretching and flat plate surfaces. Prabhavathi et al. [20], Sudarsana Reddy and Chamkha [21], and Swarnalathamma [22] simultaneously examined the phenomenon of free convection in nanofluids, taking into account the influence of MHD and chemical processes. Samuel Olumide Adesanya et al. [23], Saima Noreen [24], and Abdul Samad Khan et al. [25] conducted numerical investigations on non-Newtonian fluid flow with the influence of MHD and convective boundary conditions. Sambath et al. [26] elucidated the utilization of thermal radiation in free convection flow over vertical cones and observed an increase in heat dissipation due to thermal radiation effects. Numerical studies were conducted by Asha Shivappa Kotnurkar and Sunitha Giddaiah [27], Anantha Kumar et al. [28], and Subharthi Sarkar and Mehari Fentahun Endalew [29] to investigate the flow of non-Newtonian fluids under natural convection, considering the influence of magnetohydrodynamics (MHD), radiant heat, and chemical processes. Various researchers [30–33] investigated the impact of microorganisms in natural convection flow problems under different boundary conditions. Muhammad Bilal and Samia Ashbar [34] and Gangadhar Kotha et al. [35] delved into non-Newtonian fluid flow in mixed convection problems with the influence of microorganisms. Basha and Sivaraj [36], Wei-Feng Xia et al. [37], and Fazal Haq [38] investigated the flow of non-Newtonian nanofluids over various geometries, considering the influence of magnetohydrodynamics (MHD) to improve the dispersion of heat and mass. Various boundary conditions were considered by several scholars [39–41] in their investigations of the heat and mass transfer aspects of forced and free convection problems. Numerical studies on the flow of non-Newtonian fluids across stretching surfaces with the impact of MHD were undertaken by Ijaz Khan et al. [42] and Bharatkumar Manvi et al. [43]. Various authors [44–47] numerically investigated Eyring-Powell fluid flow over different geometries, including MHD, thermal radiation, and mixed boundary conditions. Some researchers [48–51] theoretically examined non-Newtonian nanofluid flow over various geometries with the effects of MHD. Kotha Gangadhar et al. [52], Susmay Nandi et al.
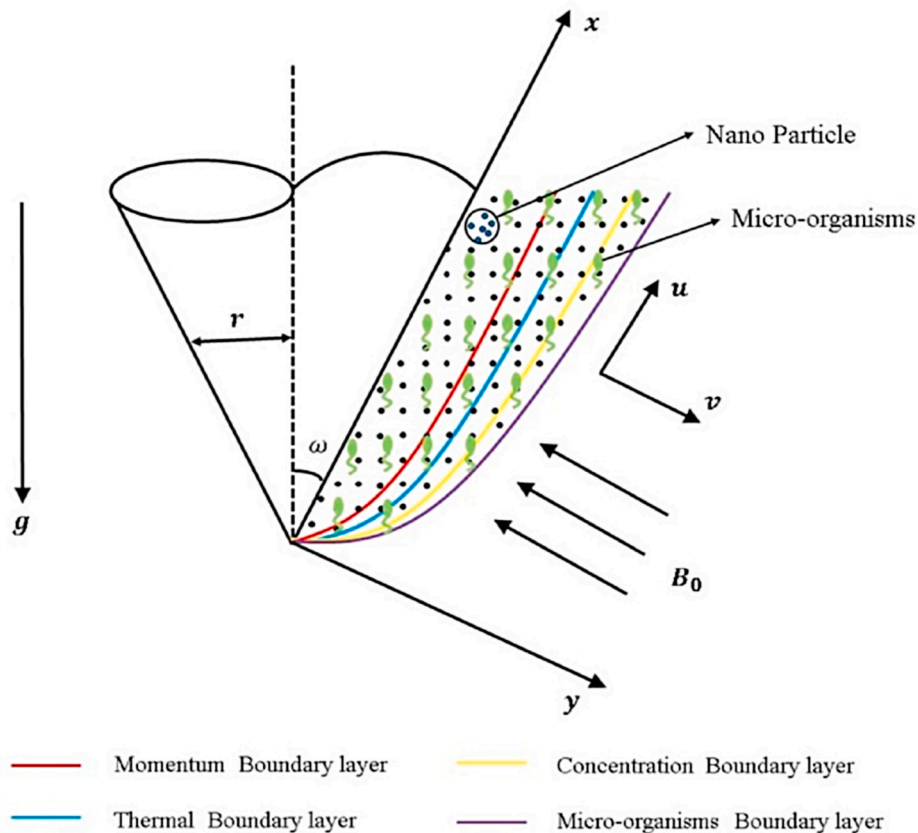

Fig. 1. Physical model.

[53], and Mandal et al. [54] investigated nanofluid flow in various geometries using different nanoparticles for distinct heat and mass transfer purposes. In their respective studies, Muhammad Sohail Khan et al. [55], Kotha Gangadhar et al. [56], and Dhanekula Naga Bhargavi et al. [57] discovered that hybrid nanofluids outperform single-based nanofluids in terms of enhancing mass and thermal transfer in convection concerns. Several authors [58–61] conducted numerical examinations of bio-convection fluid flow problems on various geometries with different boundary conditions. Multiple researchers [62–66] conducted numerical investigations. They observed that thermal radiation and MHD effects enhance heat transfer, yielding superior results in non-Newtonian nanofluid flow compared to normal fluids over various geometries. Patil et al. [67–71] examined the behavior of a non-Newtonian fluid model under convective boundary situations and evaluated it numerically by employing the finite difference quasilinearization method. Additionally, Patil et al. [72–76] looked at the mass and heat transfer of various geometries and diverse nanoparticle types.

The main objective of this study is to examine the movement of nanofluid over an upright position cone surface, specifically focusing on the impact of Joule heating, viscous dissipation, and magnetohydrodynamics (MHD) with convective boundary conditions. It should be noted that no previous research has been conducted on this particular topic. The coefficient of convective heat transfer (h_f) is a crucial variable that quantifies the rate at which heat is transported between the conical surface and the non-Newtonian fluid. Given the circumstances, we are presented with a cone that has undergone heating and now requires cooling. In order to accomplish this, we employ a water-based nanofluid that contains microorganisms. The cone is immersed in a specifically engineered non-Newtonian nanofluid containing microorganisms. This configuration offers a stimulating structure to support biotechnological investigation. Every element of this system has a crucial function in the complex mechanisms of heat and mass transport, providing a diverse array of practical uses.

The remaining sections of the paper are shown below: The problem's boundary circumstances, mathematical model, and governing equation can be addressed in Section 2. The methodology for resolving the governing equation is discussed in Section 3. Section 4 uses visuals to effectively present and explain the findings. Section 5 provided a series of final observations on the subject being examined.

2. Mathematical formulation of the model

The motion of an Eyring-Powell nanofluid that is incompressible, 2D, and steady across an upright cone in the occurrence of MHD and viscous dissipation is considered. The parameter r represents the cone's radius, and the parameter ω represents its half-angle. The y-axis is orthogonal to the surface of the cone, whereas the x-axis parallels the surface of the cone as it moves along it. u and v, respectively, represent the velocity components along the *x*- and *y*-axes. The present mathematical model of the system is depicted in Fig. 1. In the current steady-state analysis, we ignore the effects of the induced magnetic field and currents. Consider that all the characteristics of the fluid remain constant, with the exception of density. Equations for velocity, thermal, continuity, concentration, and density of microorganisms are presented here. The equations were derived through the use of the Boussinesq approximation [42–47].

Equation of Continuity

$$\frac{\partial(ru)}{\partial x} + \frac{\partial(rv)}{\partial y} = 0 \tag{1}$$

Equation of Momentum

$$(\rho_{nf})\left(u\frac{\partial u}{\partial x} + v\frac{\partial u}{\partial y}\right)$$
$$= \left(-\frac{1}{2\beta d^3}\left(\frac{\partial u}{\partial y}\right)^2\right)\left(\frac{\partial^2 u}{\partial y^2}\right) - \frac{\mu_{nf}}{k_1}.u - \sigma_1(B_0)^2 u$$
$$+\left((\rho\beta_T)_{nf}(T - T_\infty) + (\rho\beta_C)_{nf}(C - C_\infty)\right)g\cos\omega \tag{2}$$
$$+\left(\gamma(\rho\beta_N)_{nf}\Delta\rho(N - N_\infty)\right)g\cos\omega$$
$$+\left(\mu_{nf} + \frac{1}{\beta d}\right)\left(\frac{\partial^2 u}{\partial y^2}\right)$$

Equation of Energy

$$u\frac{\partial T}{\partial x} + v\frac{\partial T}{\partial y} = \alpha_{nf}\frac{\partial^2 T}{\partial y^2} + \frac{\mu_{nf}}{(\rho c_p)_{nf}}\left(\frac{\partial u}{\partial y}\right)^2 + \frac{\sigma B_0^2}{(\rho c_p)_{nf}}u^2 \tag{3}$$

Equation of Concentration

$$u\frac{\partial C}{\partial x} + v\frac{\partial C}{\partial y} = D\frac{\partial^2 C}{\partial y^2} \tag{4}$$

Equation of Microorganisms

$$u\frac{\partial N}{\partial x} + v\frac{\partial N}{\partial y} + \frac{bW_c}{(C_w - C_\infty)}\frac{\partial}{\partial y}\left(N\frac{\partial C}{\partial y}\right) = D_n\frac{\partial^2 N}{\partial y^2} \tag{5}$$

Boundary condition (BC) are

$$u = 0, v = 0, -k_{nf}\frac{\partial T}{\partial y} = h_f(T_w - T), C = C_w, N = N_w \quad at \quad y = 0 \tag{6}$$

$$u \to 0, T \to T_\infty, C \to C_\infty, N \to N_\infty \quad as \quad y \to \infty$$

The equations for density (ρ), heat capacity (c_p), and thermal expansion coefficient $(\overline{\beta})$ in nanofluids are provided, and Table 1 gives the thermo-physical properties of nanofluids that have been taken in the current model.

$$\alpha_{nf} = \frac{k_{nf}}{(\rho c_p)_{nf}}, \mu_{nf}(1-\varphi)^{2.5} = \mu_f,$$

$$\rho_{nf} - \varphi\rho_s = (1-\varphi)\rho_f, (\beta\rho)_{nf} - \varphi(\beta\rho)_s = (1-\varphi)(\beta\rho)_f$$

$$(\rho c_p)_{nf} - \varphi(\rho c_p)_s = (1-\varphi)(\rho c_p)_f, \frac{k_{nf}}{k_f} = \frac{k_s + (n-1)k_f - 2\varphi(k_f - k_s)}{(k_s + (n-1)n - 1)k_s + k_f + \varphi(k_f - k_s)}$$

Consider the stream function $\Psi(x,y)$ and $u = \frac{1}{r}\frac{\partial\Psi}{\partial y}$ and $v = \frac{1}{r}\frac{\partial\Psi}{\partial x}$ are defined. Then, by applying the corresponding similarity transformations, a set of non-linear ODEs can be derived from the controlling non-linear partial differential equations (1)–(6). The similarity variables are given by,

$$v = \frac{\nu_f}{4x}(Gr)^{1/2}[\xi.f'(\Psi) - 7f(\xi)], \xi = \frac{y}{x}(Gr)^{1/4}, u = \frac{\nu_f}{x}(Gr)^{1/4}.f'(\xi),$$

$$\theta(\xi) = \frac{T - T_\infty}{T_w - T_\infty}, Gr = \frac{g\beta_T(T_w - T_\infty)cos\,\omega.x^3}{\nu_f^2}, \varphi(\xi) = \frac{C - C_\infty}{C_w - C_\infty}, \chi(\xi) = \frac{N - N_\infty}{N_w - N_\infty},$$

$$r = sin\,\omega, \Psi = \nu_f r(Gr)^{1/4}.f(\xi),$$

By utilizing similarity variables, we achieve the satisfaction of the continuity equation. Subsequently, we express the momentum, thermal, concentration, and microbial in non-dimensional form by employing similarity transformations.

$$\left(\frac{1}{A_2}\right)(A_1 + K - KN_1(f'')^2)f''' - \left(\frac{\Gamma}{A_2}\right)\left(A_1 + K - \frac{KN_1}{3}(f'')^2\right)f' - \left(\left(\frac{1}{2}\right)f'^2 - \left(\frac{7}{4}\right)ff''\right) + A_3(\theta + N_r\,\varphi + R_b\,\chi) - \frac{M}{A_2}f' = 0 \tag{7}$$

$$\frac{A_4}{P_r}\left(\frac{k_{nf}}{k_f}\right)\theta'' + \left(\frac{7}{4}\right)f\theta' + \left(A_1 + K - \frac{KN_1}{3}(f'')^2\right)A_4Ec(f'')^2 + A_4J_u(f')^2 = 0 \tag{8}$$

$$\left(\frac{1}{S_c}\right)\varphi'' + \left(\frac{7}{4}\right)f\varphi' = 0 \tag{9}$$

$$\chi'' + \left(\frac{7}{4}\right)L_bf\chi' - P_e(\chi'\varphi' + (\chi + \sigma)\varphi'') = 0 \tag{10}$$

The Corresponding BC's are

$$f = 0, \quad f' = 0, \frac{k_{nf}}{kf}\theta' = -B_1(1 - \theta), \varphi = 1, \chi = 1 \; at \; \xi = 0 \tag{11}$$

$$f'(\xi) \to 0, \theta(\xi) \to 0, \varphi(\xi) \to 0, \chi(\xi) \to 0 \quad as \quad \xi \to \infty$$

Table 1
Thermo-physical properties of water and nanoparticle.

Fluid	$\rho\left(\frac{Kg}{m^3}\right)$	$Cp\left(\frac{J}{kgK}\right)$	$k\left(\frac{W}{mK}\right)$	$\overline{\beta} \times 10^{-5}(K^{-1})$
H_2O	997.1	4179	0.613	21
Cu	8933	385	401	1.67
Ag	10,500	235	429	1.89
Al_2O_3	3970	765	40	0.85
TiO_2	4250	686.2	8.9538	0.9

where,

$$K = \left(\frac{1}{\mu_f d\beta}\right), N_1 = \frac{\nu_f^2 (\text{Gr})^{\frac{3}{2}}}{2d^2 x^4}, N_r = \frac{\beta_C (C_w - C_\infty)}{\beta_T (T_w - T_\infty)}, R_b = \frac{\beta_N (N_w - N_\infty)\Delta\rho\gamma}{\beta_T (T_w - T_\infty)}, S_c = \frac{\nu_f}{D}, Pr = \frac{\nu_f}{\alpha_f},$$

$$L_b = \frac{\nu_f}{D_n}, \Gamma = \frac{(Gr)^{-1/2} x^2}{k_1}, M = \frac{\sigma_1 . B_0^2 (Gr)^{-1/2} x^2}{\mu_f}, P_e = \frac{bW_c}{D_n}, \sigma = \frac{N_\infty}{N_w - N_\infty}, E_c = \frac{\nu_f^2 Gr^{1/4}}{(c_p)_f x^2 (T_w - T_\infty)},$$

$$B_1 = \frac{h_f x}{Gr^{1/4} k_f}, A_1 = \frac{1}{(1 - \varphi)^{2.5}}, A_2 = 1 - \varphi + \varphi\left(\frac{\rho_s}{\rho_f}\right), A_3 = \frac{1 - \varphi + \varphi\left(\frac{(\rho\beta)_s}{(\rho\beta)_f}\right)}{1 - \varphi + \varphi\left(\frac{\rho_s}{\rho_f}\right)},$$

$$A_4 = \frac{1}{1 - \varphi + \varphi\left(\frac{(\rho c_p)_s}{(\rho c_p)_f}\right)}, J_u = \frac{\sigma B_0^2}{(\rho c_p)_f} \nu_f (Gr)^{\frac{-1}{4}}.$$

The local skin friction coefficient C_f, local Nusselt factor N_u, local Sherwood factor S_h, and local microbial density value N_n are all provided below in their non-dimensional versions.
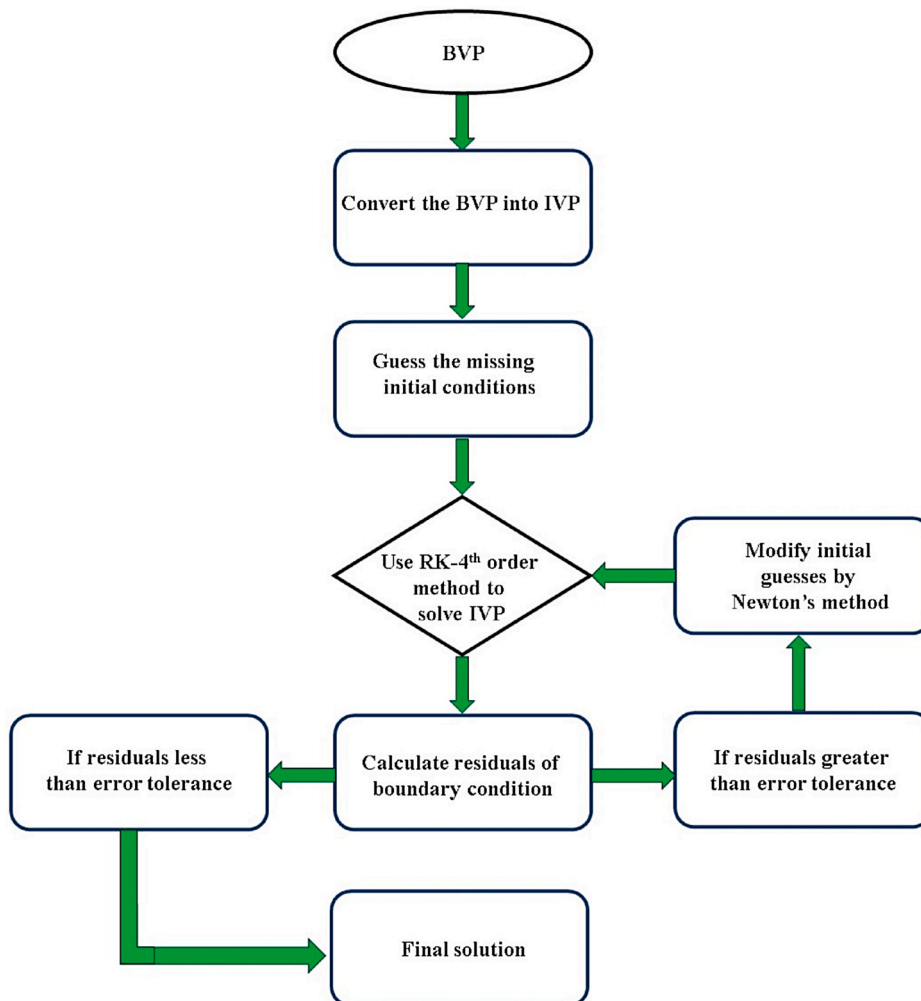

Fig. 2. Flow chart of shooting method.

$$(Gr)^{1/4}C_f = (A_1 + K)f''(0) - \frac{KN_1}{3}\left(f'(0)^3\right), (Gr)^{-1/4}Nu = \frac{-k_{nf}}{k_f}\theta'(0)$$

$$(Gr)^{-1/4}Sh = -\varphi'(0), \quad (Gr)^{-1/4}Nn = -\chi'(0)$$

3. Computational analysis

The numerical solution for equations 7–10, incorporating boundary condition (11), can be obtained by reducing equations 7–10 into a system of first-order differential equations under the assumption that $f = z_1, f' = z_2, f'' = z_3, \theta = z_4, \theta' = z_5, \varphi = z_6, \varphi' = z_7, \chi = z_8, \chi' = z_9$.

$$f'' = \left[\frac{\left(\left(\frac{1}{2}\right)z_2^2 - \left(\frac{7}{4}\right)z_1z_3\right) + \left(\frac{\Gamma}{A_2}\right)\left(A_1 + K - \frac{KN_1}{3}(z_3)^2\right)z_2 + A_3(z_4 - N_rz_6 - R_bz_8) + \frac{M}{A_2}z_2}{\left(\frac{1}{A_2}\right)\left(A_1 + K - KN_1(z_3)^2\right)}\right]$$

$$\theta'' = \left[\frac{\left(-\frac{7}{4}\right)z_1z_5 - \left(A_1 + K - \frac{KN_1}{3}(z_3)^2\right)A_4Ec.z_3^2 - A_4J_u(z_2)^2}{\left(\frac{1}{\Pr}\right)A_4\left(\frac{k_{nf}}{k_f}\right)}\right]$$

$$\varphi'' = \left[\left(\left(-\frac{7}{4}\right)z_1z_7\right)S_c\right]$$

$$\chi'' = \left[\left(\frac{7}{4}\right)L_bz_1z_9 + P_e\left(z_9z_7 + (z_8 + \sigma)\left[\left(\left(-\frac{7}{4}\right)z_1z_7\right)S_c\right]\right)\right]$$

with BCs, $z_1 = 0, z_2 = 0, z_3 = U_1, \frac{k_{nf}}{kf}z_5 = -B_1(1 - z_4), z_5 = U_2, z_6 = 1, z_7 = U_3,$

$z_8 = 1, z_9 = U_4$. These U_1, U_2, U_3 and U_4 values all represent unknown boundary conditions (BCs). We need to use the shooting technique to locate the appropriate boundary values to obtain a solution for the first-order differential equation presented earlier. The margin of error for the undetermined boundary values that were measured at the point 10^{-6}. The solution of the first-order ordinary differential equations system was accomplished successfully using the Bvp4c function in MATLAB. Fig. 2 explains the shooting technique and how it functions in detail. The present study's findings are corroborated by comparing them to the prior research conducted by Hamad [17]. The comparison of the two comparable results is presented in Table 2, which also provides validation for the current numerical techniques.

4. Result and findings

In this simulation, the bio-convective fluid flow's mass and heat transfer are visually demonstrated. Four distinct types of nano-particles: copper (Cu), aluminum oxide (Al_2O_3), titanium dioxide (TiO_2), and silver (Ag), along with three different volume fractions of 0.01, 0.02 and 0.03 will be used to explore the impact of nanofluid on heat and mass transmission. The choice of our values is made with a view to focus bio-convection. Thus, our model will enhance the heat and mass transfer to an optimal level. All parameter value ranges in this model were chosen in the ways shown below. $0.01 \leq \varphi \leq 0.03, 0 \leq K \leq 0.3, 1 \leq \Gamma \leq 3, 1 \leq M \leq 3, 0.3 \leq E_c \leq 0.9, 1 \leq B_1 \leq 3, 0.5 \leq S_c = 1.5, 0.3 \leq N_r \leq 0.7, 1 \leq P_r \leq 6.2, 0.5 \leq L_b \leq 1, 0.1 \leq P_e \leq 0.5, 0.3 \leq R_b \leq 0.9, 1 \leq J_u \leq 3$. In Figs. 3–26, we

Table 2
Comparison of previous results with the present, while maintaining $\varphi = 0.1, Nr = Rb = \Gamma = E_c = L_b = P_e = S_c = K = N_1 = B_1 = J_u = 0.$

| local skin friction								
M	Cu		Ag		Al₂O₃		TiO₂	
	Hamad [17]	Present	Hamad [17]	Present	Hamad [17]	Present	Hamad [17]	Present
0	1.17475	1.17476	1.22507	1.2251	0.99877	0.99878	1.00952	1.00951
0.5	1.32825	1.32825	1.37296	1.37296	1.17548	1.17548	1.18463	1.1846
1	1.46576	1.46575	1.5064	1.5065	1.3289	1.3291	1.337	1.3371
2	1.70789	1.7079	1.74289	1.7429	1.59198	1.59199	1.59875	1.5988
local Nusselt number								
0	1.45207	1.4521	1.42058	1.42057	1.4917	1.4917	1.51959	1.5196
0.5	1.41848	1.4185	1.38824	1.38825	1.45299	1.45299	1.48124	1.4813
1	1.38847	1.38848	1.35917	1.35918	1.41942	1.41942	1.44788	1.44789
2	1.336	1.3361	1.30808	1.3081	1.36212	1.36212	1.39085	1.39086
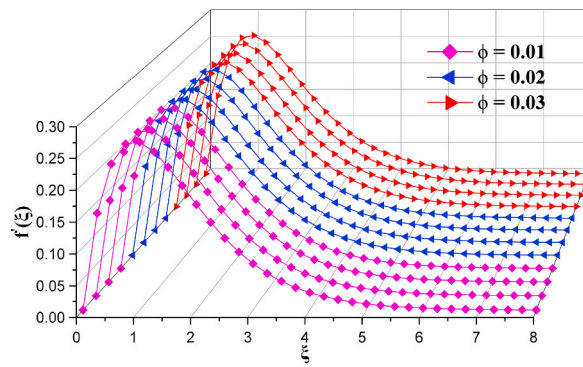
Fig. 3. Impact of φ over velocity when $K = 0.3, \Gamma = 1, M = 0.6, E_c = 0.3, B_1 = 1, S_c = 1, N_r = 0.5, L_b = 0.7, P_e = 0.3, R_b = 0.3, P_r = 6.2, J_u = 1$.
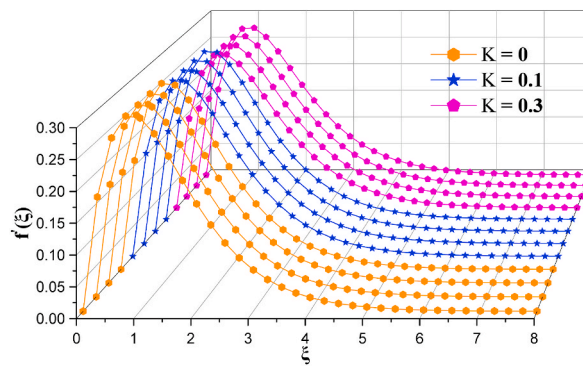

Fig. 4. Impact of K on velocity when $\varphi = 0.01, \Gamma = 1, M = 0.6, E_c = 0.3, B_1 = 1, S_c = 1, N_r = 0.5, L_b = 0.7, P_e = 0.3, R_b = 0.3, P_r = 6.2, J_u = 1$.
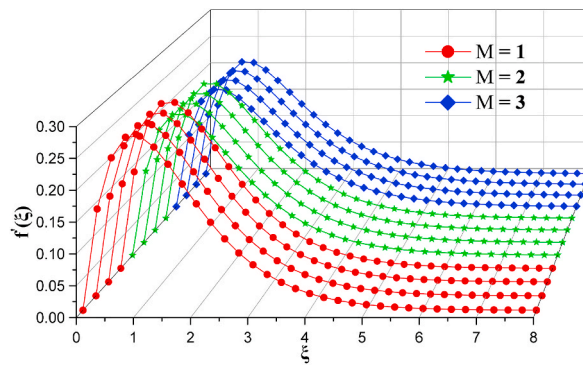

Fig. 5. Impact of M on velocity when $\varphi = 0.01, \Gamma = 1, K = 0.3, E_c = 0.3, B_1 = 1, S_c = 1, N_r = 0.5, L_b = 0.7, P_e = 0.3, R_b = 0.3, P_r = 6.2, J_u = 1$.

have three blocks containing four curves bearing the same color and pattern. Further, in each block, the first curve represents *Cu*, the second stands for *Ag*, the third one corresponds to Al_2O_3 and the fourth curve in each block represents TiO_2.

4.1. Velocity profile

Fig. 3 displays the velocity profiles of different water-based nanofluids at varying volume fractions (φ), revealing an inverse relationship between velocity and volume fraction. Fig. 4 shows that the velocity profile is reduced (4 %) when the Powell-Eyring fluid characteristic parameter (K) is increased.

Also, as seen in Fig. 5, the velocity profile drops (23 %) and the MHD parameter (M) rises due to the tangential Lorentz force that
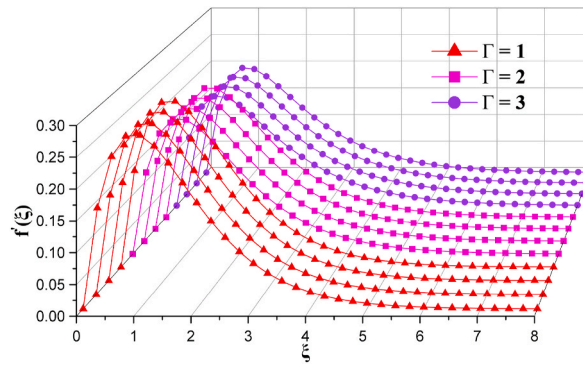
Fig. 6. Impact of Γ on velocity when $\varphi = 0.01, M = 0.6, K = 0.3, E_c = 0.3, B_1 = 1, S_c = 1, N_r = 0.5, L_b = 0.7, P_e = 0.3, R_b = 0.3, P_r = 6.2, J_u = 1$.
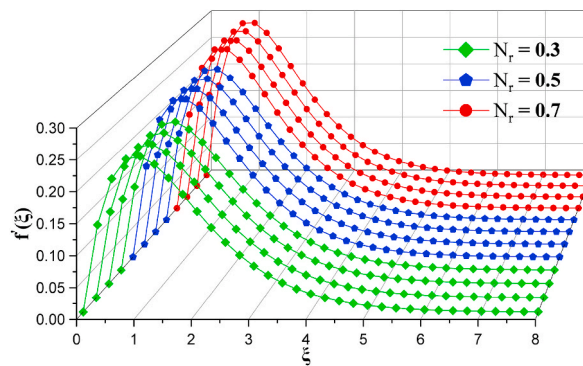

Fig. 7. Impact of N_r on velocity when $\varphi = 0.01, M = 0.6, K = 0.3, E_c = 0.3, B_1 = 1, S_c = 1, \Gamma = 1, L_b = 0.7, P_e = 0.3, R_b = 0.3, P_r = 6.2, J_u = 1$.
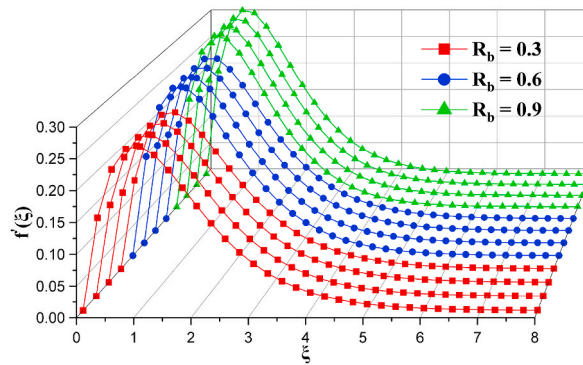

Fig. 8. Impact of R_b over velocity when $\varphi = 0.01, M = 0.6, K = 0.3, E_c = 0.3, B_1 = 1, S_c = 1, \Gamma = 1, L_b = 0.7, P_e = 0.3, N_r = 0.5, P_r = 6.2, J_u = 1$.

impacts on the flow of the fluid. The momentum boundary layer around the cone thickens due to this force. A thicker momentum barrier layer (22%) is obtained by increasing the porosity parameter (Γ), as Fig. 6 illustrates. The drag force acting on a cone surface depends on its porosity; more porous surfaces reduce drag by permitting fluid to travel through the cone rather than divert around it. Figs. 7 and 8 demonstrate that increasing the buoyancy ratio factor (N_r) and bio-convection Rayleigh number (R_b) results in an enhancement of the velocity profile for cone surfaces. Hence, an increase in this parameter augments momentum transfer within the fluid. The skin friction coefficient (C_f), quantifies the frictional drag experienced by a fluid as it flows over a cone surface. It is an indicator of the shear stress exerted by the fluid on the surface. The data presented in Table 3 demonstrates that the skin friction number increases with higher values of the volume fraction (φ), Powell-Eyring fluid factor (K), buoyancy ratio factor (N_r), and bio-convection Rayleigh number (R_b). In contrast, raising the values of the Magnetic parameter (M) and porosity parameter (Γ)
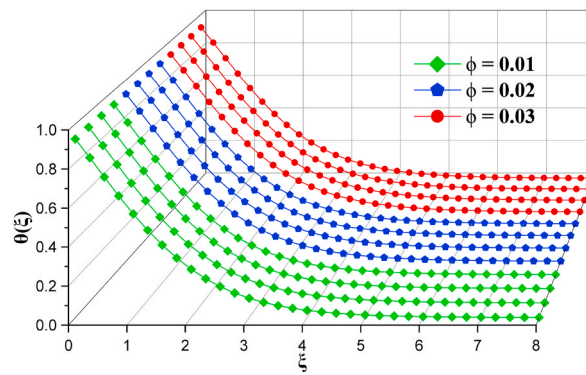
Fig. 9. Impact of φ on thermal when $R_b = 0.3, M = 0.6, K = 0.3, E_c = 0.3, B_1 = 1, S_c = 1, \Gamma = 1, L_b = 0.7, P_e = 0.3, N_r = 0.5, P_r = 6.2, J_u = 1$.

Fig. 10. Impact of K on thermal when $R_b = 0.3, M = 0.6, \varphi = 0.01, E_c = 0.3, B_1 = 1, S_c = 1, \Gamma = 1, L_b = 0.7, P_e = 0.3, N_r = 0.5, P_r = 6.2, J_u = 1$.
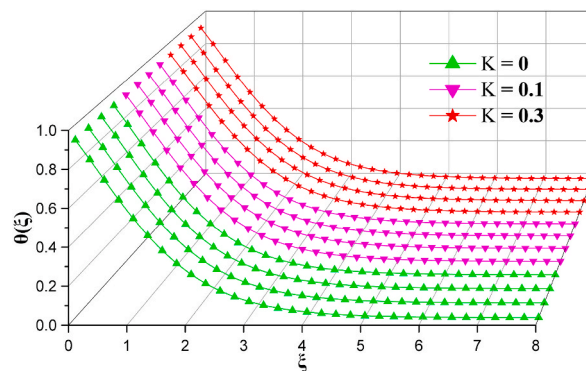

Fig. 11. Impact of M on thermal when $R_b = 0.3, K = 0.3, \varphi = 0.01, E_c = 0.3, B_1 = 1, S_c = 1, \Gamma = 1, L_b = 0.7, P_e = 0.3, N_r = 0.5, P_r = 6.2, J_u = 1$.
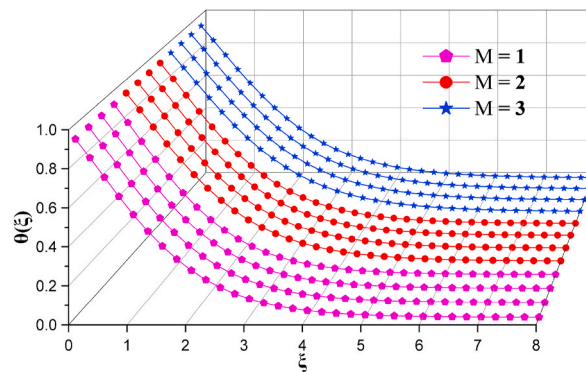
reduces the skin friction number, facilitating a more efficient fluid flow across the cone. Among all nanofluids, titanium (TiO_2) demonstrates the minimum skin friction number when the Magnetic and porosity parameters are increased.

4.2. Temperature profile

Figs. 9–15 provide temperature profiles for different dimensionless parameters, including volume fraction (φ) of nanofluid, Powell-Eyring fluid parameter (K), MHD (M), Porosity (Γ), viscous dissipation parameter (E_c), Prandtl number (P_r) and Joule heating parameter (J_u). Fig. 9 demonstrates that increasing the volume fraction (φ) leads to higher temperature profiles, indicating improved
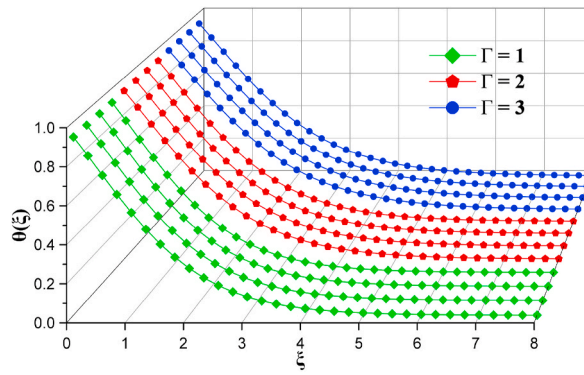
Fig. 12. Impact of Γ on thermal when $R_b = 0.3, K = 0.3, \varphi = 0.01, E_c = 0.3, B_1 = 1, S_c = 1, M = 0.6, L_b = 0.7, P_e = 0.3, N_r = 0.5, P_r = 6.2, J_u = 1$.
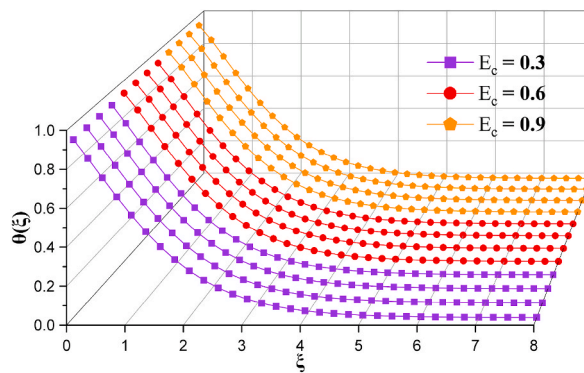

Fig. 13. Impact of E_c on thermal when $R_b = 0.3, K = 0.3, \varphi = 0.01, \Gamma = 1, B_1 = 1, S_c = 1, M = 0.6, L_b = 0.7, P_e = 0.3, N_r = 0.5, P_r = 6.2, J_u = 1$.
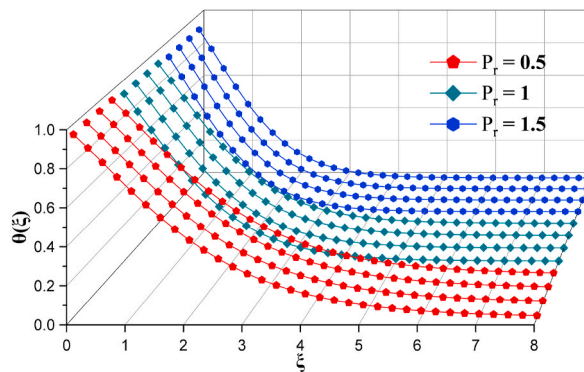

Fig. 14. Impact of P_r on thermal when $R_b = 0.3, K = 0.3, \varphi = 0.01, \Gamma = 1, E_c = 0.3, B_1 = 1, S_c = 1, M = 0.6, L_b = 0.7, P_e = 0.3, N_r = 0.5, J_u = 1$.

heat transfer rates (3.5 %) with a higher nanofluid concentration.

Fig. 10 illustrates the importance of the Powell-Eyring fluid factor (K) also indicates that increasing it leads to a boost (3 %) in heat transmission. Increasing the MHD parameter (M) enhances heat transfer (19 %) by taking advantage of the interaction between the fluid's moving charged particles and a magnetic field, as shown in Fig. 11. With an emphasis on the greater surface area available for heat exchange in porous material, Fig. 12 focuses on the relationship between porosity (Γ) and heat transfer. The effects of raising the viscous dissipation parameter (E_c), which result in an increase in temperature, a redistribution of energy, and improved heat transfer processes (8 %), are depicted in Fig. 13. Fig. 14 presents temperature profiles for different Prandtl parameters (P_r), which describe momentum and thermal diffusion rates. In Fig. 15, the Joule heating parameter (J_u) is elucidated. The figure illustrates that as the
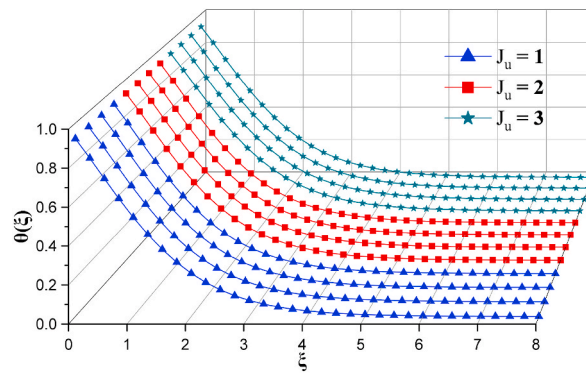
Fig. 15. Impact of J_u on temperature when $R_b = 0.3, K = 0.3, \varphi = 0.01, \Gamma = 1, B_1 = 1, E_c = 0.3, S_c = 1, M = 0.6, L_b = 0.7, P_e = 0.3, N_r = 0.5, P_r = 6.2$.
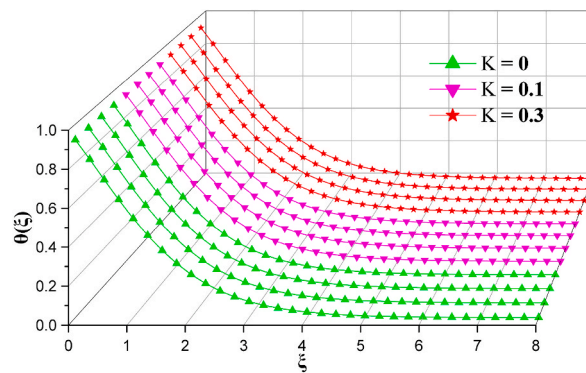

Fig. 16. Impact of φ on concentration when $R_b = 0.3, J_u = 1, \varphi = 0.01, \Gamma = 1, B_1 = 1, E_c = 0.3, S_c = 1, M = 0.6, L_b = 0.7, P_e = 0.3, N_r = 0.5, P_r = 6.2$.

Fig. 17. Impact of K on concentration when $R_b = 0.3, J_u = 1, K = 0.3, \Gamma = 1, B_1 = 1, S_c = 1, M = 0.6, L_b = 0.7, P_e = 0.3, E_c = 0.3, N_r = 0.5, P_r = 6.2$.

Joule heat coefficient (J_u) rises, the thickness of the thermal boundary layer decreases to its minimal value. This implies that thermal diffusion (21 %) occurs rapidly. Joule heating in steady-state heat transfer describes the continuous generation of heat on the cone surface due to electrical current passing through it. Heat transfer mechanisms must balance this heat to maintain a steady temperature distribution. The Nusselt number (N_u) determines the heat transfer rate from a cone surface to a fluid. This is a clear indication of the efficiency of heat transmission. Table 4 indicates that copper (Cu) and aluminum (Al_2O_3) exhibit better heat transfer rates compared to silver (Ag) and titanium (TiO_2) when increasing the volume fraction (φ), MHD (M), porosity parameter (Γ), Joule heating parameter (J_u), and viscous dissipation parameter (E_c). These figures and tables provide valuable insights for optimizing heat transfer rates in various applications.
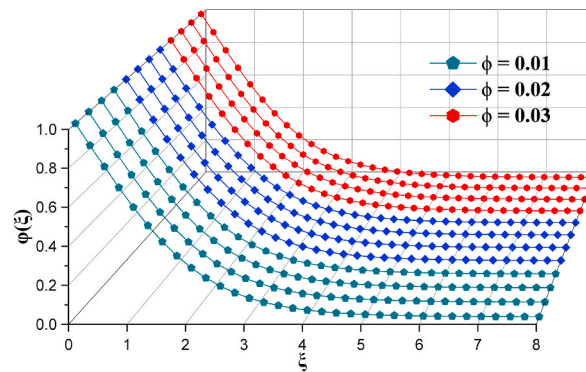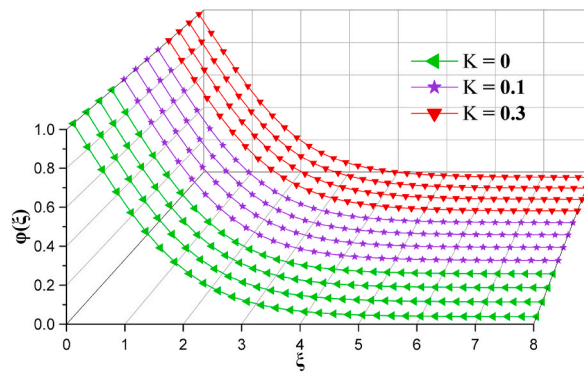
Fig. 18. Impact of M on concentration when $R_b = 0.3, J_u = 1, \varphi = 0.01, \Gamma = 1, B_1 = 1, S_c = 1, M = 0.6, L_b = 0.7, P_e = 0.3, E_c = 0.3, N_r = 0.5,$ $P_r = 6.2.$
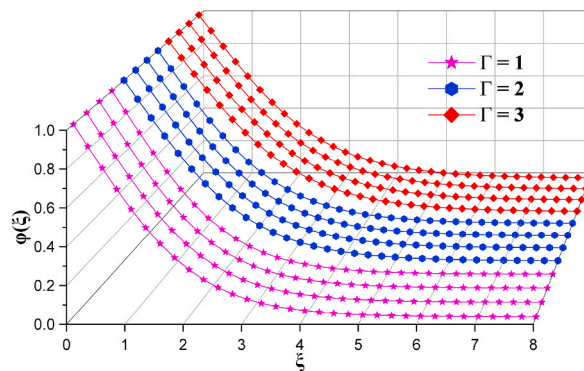
Fig. 19. Impact of Γ on concentration when $R_b = 0.3, J_u = 1, \varphi = 0.01, K = 0.3, B_1 = 1, S_c = 1, M = 0.6, L_b = 0.7, P_e = 0.3, N_r = 0.5, E_c = 0.3, P_r = 6.2.$
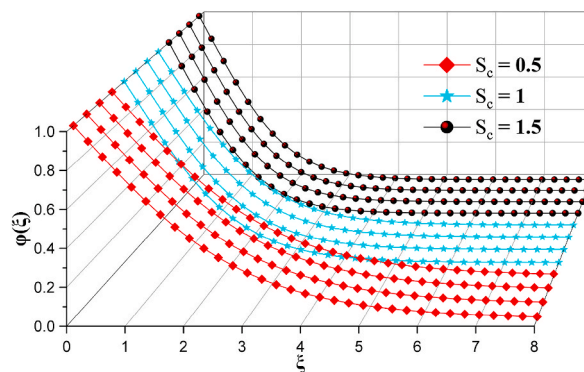
Fig. 20. Impact of S_c on concentration when $R_b = 0.3, J_u = 1, \varphi = 0.01, K = 0.3, B_1 = 1, \Gamma = 1, M = 0.6, L_b = 0.7, P_e = 0.3, N_r = 0.5, E_c = 0.3, P_r = 6.2.$

4.3. Concentration profile

Figs. 16–20 provide insightful concentration profiles for various dimensionless parameters, including volume fraction (φ) of nanofluid, Powell-Eyring fluid parameter (K), MHD (M), porosity parameter (Γ), and Schmidt number (S_c). As seen in Fig. 16, nanoparticles that obstruct molecular motion and alter transport characteristics are responsible for the greater concentration diffusion rate resulting from raising the volume fraction (φ). Fig. 17 demonstrates that a slight enhancement in the Powell-Eyring liquid factor (K) impacts the combining and dispersion of the fluid, hence influencing concentration profiles by an increase (3%) in the rate of concentration spread, attributed to an elevated stress tensor. The impact of mass transfer efficiency and concentration boundary layer

Fig. 21. Impact of K on microorganism when $R_b = 0.3, J_u = 1, \varphi = 0.01, S_c = 1, B_1 = 1, \Gamma = 1, M = 0.6, L_b = 0.7, P_e = 0.3, N_r = 0.5, E_c = 0.3, P_r = 6.2$.

Fig. 22. Impact of M on microorganism when $R_b = 0.3, J_u = 1, \varphi = 0.01, S_c = 1, B_1 = 1, \Gamma = 1, K = 0.3, L_b = 0.7, P_e = 0.3, E_c = 0.3, N_r = 0.5, P_r = 6.2$.

Fig. 23. Impact of Γ on microorganism when $R_b = 0.3, J_u = 1, \varphi = 0.01, S_c = 1, B_1 = 1, M = 0.6, K = 0.3, L_b = 0.7, P_e = 0.3, N_r = 0.5, E_c = 0.3, P_r = 6.2$.

thickness on MHD and an increased MHD parameter (M) is examined in Fig. 18. MHD can enhance the mass transfer process (18 %) by improving fluid mixing.

Fig. 19 indicates the influence of permeability and a higher porosity parameter (Γ) on the thickness of the concentration boundary layer. Enhancing mass transfer (15 %) through improved fluid mixing is the porosity parameter (Γ). Fig. 20 presents concentration profiles for different Schmidt numbers (S_c), which describe the relative rates of mass and momentum transfer in a fluid, with Sherwood number (S_c) indicating mass transfer efficiency. The Sherwood number (S_h) is a measure that estimates the rate at which mass is transferred from the surface of a conical structure to a fluid. This demonstrates the effectiveness of mass transfer. Table 5 demonstrates that increasing Schmidt number results in better mass transfer rates, with aluminum (Al_2O_3) and titanium (TiO_2) nanoparticles
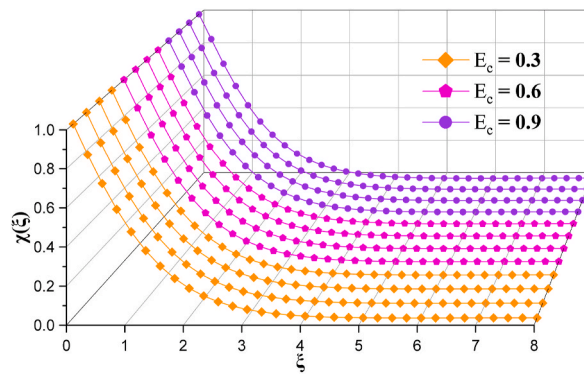
Fig. 24. Impact of E_c on microorganism when $R_b = 0.3, J_u = 1, \varphi = 0.01, S_c = 1, B_1 = 1, M = 0.6, K = 0.3, L_b = 0.7, P_e = 0.3, N_r = 0.5, P_r = 6.2$.
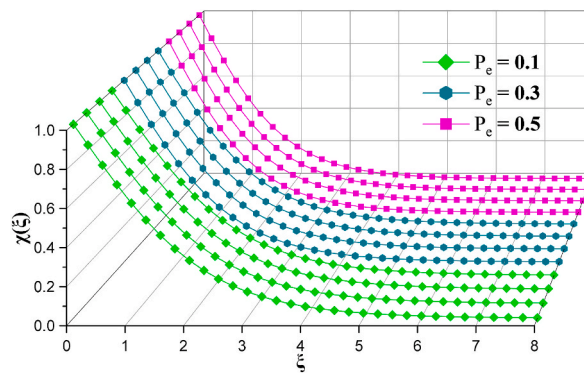
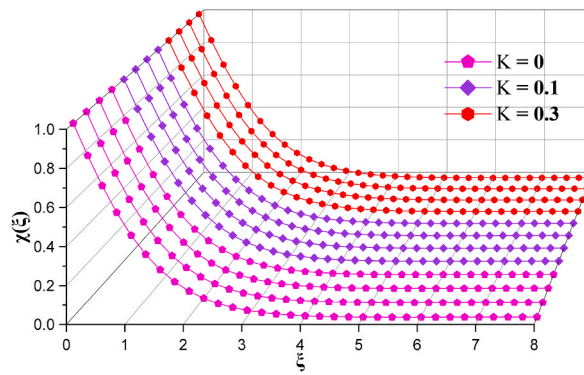
Fig. 25. Impact of P_e on microorganism when $R_b = 0.3, J_u = 1, \varphi = 0.01, S_c = 1, B_1 = 1, M = 0.6, K = 0.3, L_b = 0.7, E_c = 0.3, N_r = 0.5, P_r = 6.2$.

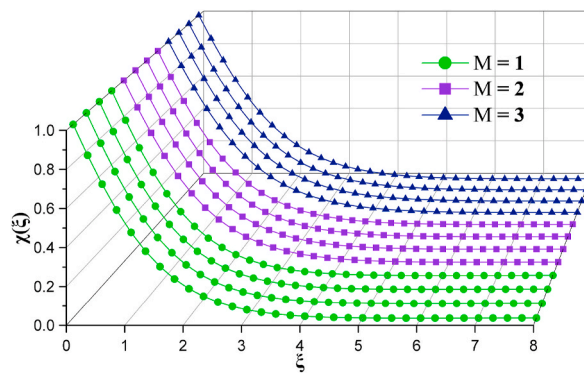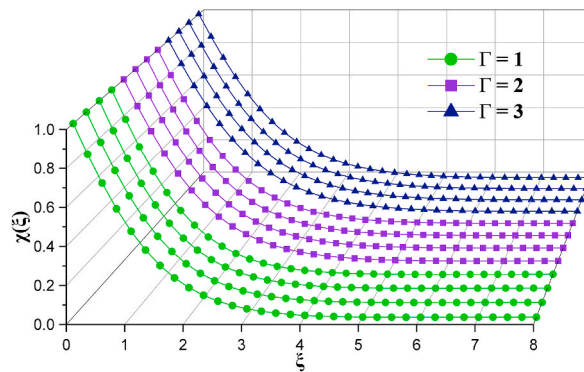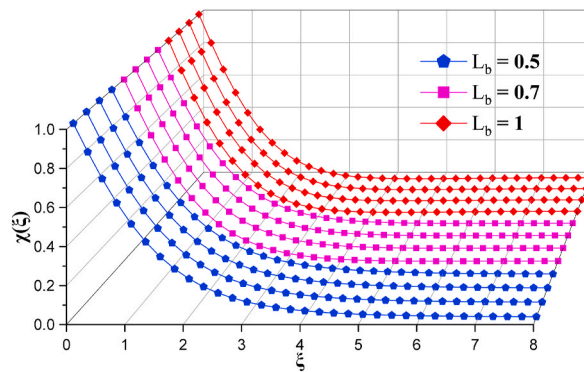**Fig. 26.** Impact of L_b on microorganism when $R_b = 0.3, J_u = 1, \varphi = 0.01, S_c = 1, B_1 = 1, M = 0.6, K = 0.3, P_e = 0.7, E_c = 0.3, N_r = 0.5, P_r = 6.2$.

exhibiting superior mass transfer compared to copper (*Cu*) and silver (*Ag*). These findings are essential for optimizing mass transfer rates in various applications.

4.4. Microorganism profile

Figs. 21–26 provide significant information about the characteristics of self-propelled microorganisms across different dimensionless parameters, such as the Powell-Eyring fluid parameter (K), MHD effects (M), porosity parameter (Γ), Lewis number (L_b), viscous dissipation parameter (E_c), and Peclet number (P_e). Fig. 21 demonstrates a positive correlation between a 4 % increase in

Table 3
Local skin friction.

φ	K	N_1	M	Γ	R_b	N_r	Cu	Ag	Al_2O_3	TiO_2
0.01	0.3	2	0.6	1	0.3	0.5	0.806685	0.80696	0.806686	0.806744
0.02							0.80619	0.806751	0.806166	0.806294
0.03							0.805495	0.806355	0.805423	0.805632
0.01	**0.1**	2	0.6	1	0.3	0.5	0.793879	0.79415	0.793941	0.794001
	0.4						0.816273	0.816552	0.81625	0.816307
	0.8						0.860841	0.861149	0.860743	0.860802
0.01	0.3	**1**	0.6	1	0.3	0.5	0.82694	0.827239	0.826938	0.827001
		2					0.806685	0.80696	0.806686	0.806744
		3					0.78524	0.785486	0.785242	0.806744
0.01	0.3	2	**0.8**	1	0.3	0.5	0.790616	0.790896	0.790574	0.790639
			1.2				0.761362	0.761646	0.761259	0.761336
			1.6				0.735352	0.735635	0.735211	0.735296
0.01	0.3	2	0.6	**1**	0.3	0.5	0.806685	0.80696	0.806686	0.806744
				2			0.716756	0.717037	0.716594	0.716684
				3			0.652714	0.652975	0.652514	0.652616
0.01	0.3	2	0.6	1	**0.1**	0.5	0.723402	0.723686	0.723372	0.723437
					0.3		0.806685	0.80696	0.806686	0.806744
					0.5		0.885383	0.885642	0.885418	0.88547
0.01	0.3	2	0.6	1	0.3	**0.3**	0.724012	0.724296	0.723985	0.724049
						0.5	0.806685	0.80696	0.806686	0.806744
						0.7	0.884769	0.885029	0.884802	0.884854

Table 4
Local Nusselt number.

φ	K	N_1	M	Γ	E_c	B_1	J_u	Cu	Ag	Al_2O_3	TiO_2
0.01	0.3	2	1	1	0.3	1	1	0.173015	0.172825	0.172979	0.172573
0.02								0.174664	0.174282	0.174589	0.173774
0.03								0.176305	0.175731	0.176187	0.174962
0.01	**0.1**	2	1	1	0.3	1	1	0.177345	0.177141	0.177335	0.176922
	0.4							0.170989	0.170804	0.170942	0.170538
	0.8							0.163773	0.163605	0.163695	0.163302
0.01	0.3	**1**	1	1	0.3	1	1	0.172738	0.172548	0.172702	0.172295
		2						0.173015	0.172825	0.172979	0.172573
		3						0.173304	0.173114	0.173268	0.172862
0.01	0.3	2	**1**	1	0.3	1	1	0.17026	0.170086	0.170201	0.169801
			2					0.163709	0.163553	0.163616	0.163235
			3					0.157921	0.157779	0.157809	0.157441
0.01	0.3	2	1	**1**	0.3	1	1	0.173015	0.172825	0.172979	0.172573
				2				0.163959	0.163796	0.163871	0.163494
				3				0.156181	0.156034	0.156068	0.155712
0.01	0.3	2	1	1	**0.1**	1	1	0.183018	0.18284	0.182987	0.182586
					0.3			0.173015	0.172825	0.172979	0.172573
					0.5			0.162553	0.16235	0.162511	0.162099
0.01	0.3	2	1	1	0.3	**0.5**	1	0.131196	0.131082	0.131171	0.130932
						0.7		0.152061	0.151912	0.152031	0.151714
						1		0.173015	0.172825	0.172979	0.172573
0.01	0.3	2	1	1	0.3	1	**1**	0.145151	0.144951	0.144997	0.144638
							2	0.114896	0.11467	0.114564	0.11425
							3	0.077392	0.07714	0.076741	0.07649

microbe diffusion rate and a small rise in the Powell-Eyring liquid factor (K). Figs. 22 and 23 illustrate the impact of magnetohydrodynamics (M) and porosity (Γ) on fluid flow, resulting in a reduction of the least boundary layer thickness and subsequently boosting the rate of microbe diffusion by 16 % and 13 % respectively. However, as Fig. 24 demonstrates, the viscous dissipation (E_c) influence on fluid flow thickens the boundary layer but does not improve the rate at which microorganisms are eradicated. Fig. 25 explores the bio-convection Peclet number (P_e) and its influence on nutrient uptake, growth, and spatial distribution of microorganisms by enhancing fluid mixing. Fig. 26 focuses on the bio-convection Lewis number (L_b), affecting pattern formation and stability of bio-convection. When the Lewis number (L_b) is higher, thermal diffusion becomes more important than mass diffusion, resulting in instability bio-convection rhythms. Table 6 indicates that increasing K, M, and Γ decreases the local microorganisms density number (N_n). Conversely, an increase in the E_c, P_e, and L_b elevates the local microorganism's density number (N_n). These findings provide valuable insights into optimizing microorganisms eradicate rates and distribution, which are crucial in various biological and biomedical applications.

Table 5
Local sherwood number.

φ	K	N_1	M	Γ	S_c	Cu	Ag	Al_2O_3	TiO_2
0.01	0.3	2	1	1	1	0.437622	0.437591	0.438082	0.437958
0.02						0.434139	0.434091	0.435018	0.434777
0.03						0.430661	0.430607	0.431917	0.431567
0.01	**0.1**	2	1	1	1	0.454717	0.454654	0.455299	0.455164
	0.4					0.42989	0.429872	0.430302	0.430183
	0.8					0.403304	0.403322	0.403577	0.403471
0.01	0.3	**1**	1	1	1	0.437278	0.437248	0.437737	0.437613
		2				0.437622	0.437591	0.438082	0.437958
		3				0.437975	0.437944	0.438437	0.438313
0.01	0.3	2	**1**	1	1	0.430043	0.430027	0.430452	0.430332
			2			0.416087	0.416094	0.416412	0.4163
			3			0.40351	0.403533	0.403771	0.403667
0.01	0.3	2	1	**1**	1	0.437622	0.437591	0.438082	0.437958
				2		0.394208	0.394241	0.394429	0.394329
				3		0.3623	0.362357	0.362413	0.362329
0.01	0.3	2	1	1	**0.5**	0.315611	0.315547	0.316073	0.315968
					1	0.437622	0.437591	0.438082	0.437958
					1.5	0.525421	0.525422	0.525834	0.525712

Table 6
Local Microorganisms density number.

φ	K	N_1	M	Γ	E_c	L_b	P_e	σ	Cu	Ag	Al_2O_3	TiO_2
0.01	0.3	2	1	1	0.3	0.7	0.5	0.1	0.427197	0.427168	0.42765	0.427528
0.02									0.423702	0.423658	0.424565	0.424328
0.03									0.420215	0.420167	0.421446	0.421102
0.01	**0.1**	2	1	1	0.3	0.7	0.5	0.1	0.444422	0.444361	0.444998	0.444865
	0.4								0.419438	0.419422	0.419842	0.419725
	0.8								0.392913	0.392932	0.393178	0.393075
0.01	0.3	**1**	1	1	0.3	0.7	0.5	0.1	0.426838	0.42681	0.42729	0.427168
		2							0.427197	0.427168	0.42765	0.427528
		3							0.427565	0.427536	0.42802	0.427898
0.01	0.3	1	**1**	1	0.3	0.7	0.5	0.1	0.413594	0.413591	0.413933	0.413827
			2						0.383891	0.383924	0.384082	0.383997
			3						0.360623	0.360671	0.360734	0.360663
0.01	0.3	2	1	**1**	0.3	0.7	0.5	0.1	0.427197	0.427168	0.42765	0.427528
				2					0.384496	0.384531	0.384706	0.38461
				3					0.353567	0.353623	0.353671	0.353592
0.01	0.3	2	1	1	**0.1**	0.7	0.5	0.1	0.425488	0.425458	0.425914	0.425798
					0.3				0.428001	0.427972	0.428436	0.42832
					0.5				0.4306	0.430574	0.431045	0.430929
0.01	0.3	2	1	1	0.3	**0.5**	0.5	0.1	0.381554	0.381519	0.381987	0.381874
						0.7			0.427197	0.427168	0.42765	0.427528
						1			0.486605	0.486591	0.487052	0.486928
0.01	0.3	2	1	1	0.3	0.7	**0.3**	0.1	0.40379	0.403755	0.404249	0.404127
							0.5		0.427197	0.427168	0.42765	0.427528
							0.7		0.449054	0.449032	0.449504	0.449381
0.01	0.3	2	1	1	0.3	0.7	0.5	**0.2**	0.437753	0.437727	0.438206	0.438083
								0.3	0.448296	0.448272	0.448748	0.448625
								0.4	0.458824	0.458802	0.459276	0.459152

5. Conclusion

This study employed computational techniques to examine the flow of bio-convective fluids along an upright cone. The investigation took into account the influence of MHD (magnetohydrodynamics), porosity, Joule heating, and viscous dissipation. The governing partial differential equations (PDEs) were converted into ordinary differential equations (ODEs) and solved numerically using MATLAB, taking advantage of shooting methods. The offered graphs reveal valuable information regarding the profiles of velocity, thermal, concentration, and microbes. Additional indications were examined, including local skin friction, local Nusselt number, local Sherwood number, and local microbe density number. Here is a list of the findings from the current investigation.

1. While increasing the volume fraction ($0.01 \leq \varphi \leq 0.03$)
   ❖ The mass and heat transfer enhanced by 3 % & 3.5 %.
2. While increasing the MHD ($1 \leq M \leq 3$), Porosity ($1 \leq \Gamma \leq 3$) parameter and Eyring-Powell fluid parameter ($0 \leq K \leq 0.3$)
   ❖ The velocity (momentum) decreased by 23 %, 22 % & 4 %.

❖The transfer of heat was enhanced by 19 %, 16 % & 3 %.
- ❖ The transfer of mass was enhanced by 18 %, 15 % & 3 %.
- ❖ The microorganism's diffusion rate was enhanced by 16 %, 13 % & 4 %.

3. While increasing the Joule heating parameter ($1 \leq J_u \leq 3$)
   - ❖ The transfer of heat was enhanced by 21 %.
4. While increasing the Viscous dissipation parameter ($0.3 \leq E_c \leq 0.9$).
   - ❖ The mass and heat transfer was enhanced by 6 % & 8 %.

6. Future direction

In the future, researchers may undertake further comprehensive examinations of the mass and heat transfer dynamics of Eyring-Powell (non-Newtonian) fluids that contain microorganisms in situations where conditions are unsteady. The existing model is limited by its incapacity to handle mixed convection within the framework of fluid flow.

Data availability statement

Data will be made available on request.
Declaration of interest's statement.
The authors declare no conflict of interest.

CRediT authorship contribution statement

P. Francis: Writing – original draft, Validation, Methodology, Formal analysis, Conceptualization. **P. Sambath:** Writing – review & editing, Validation, Software, Methodology, Formal analysis. **U. Fernandez-Gamiz:** Writing – review & editing, Validation, Methodology, Formal analysis. **S. Noeiaghdam:** Writing – review & editing, Validation, Methodology, Investigation. **S. Dinarvand:** Writing – review & editing, Validation, Methodology, Formal analysis.

Declaration of competing interest

The authors declare that they have no known competing financial interests or personal relationships that could have appeared to influence the work reported in this paper.

References

[1] A.G. Hansen, T.Y. Na, Similarity Solutions of Laminar, Incompressible Boundary Layer Equations of Non-newtonian Fluids, 1968, https://doi.org/10.1115/1.3605067.
[2] F.N. Lin, Laminar free convection from a vertical cone with Uniform surface heat Flux, Lett. Heat Mass Tran. 3 (1976) 49–58.
[3] A. Shima, T. Tsujino, The effect of Polymer concentration on the Bubble behaviour and Impulse Pressure, Chem. Eng. Sci. 36 (5) (1981) 931–935, https://doi.org/10.1016/0009-2509(81)85047-6.
[4] P Hartnett James, E.Y. Kwack, Prediction of friction and heat transfer for Viscoelastic fluids in Turbulent Pipe flow, Int. J. Thermophys. 7 (1986) 53–63, https://doi.org/10.1007/BF00503798.
[5] V. Sirohi, M.G. Timol, N.L. Kalthia, Powell-eyring model flow near an Accelerated plate, Fluid Dynam. Res. 2 (3) (1987) 193, https://doi.org/10.1016/0169-5983(87)90029-3.
[6] M. Kumari, I. Pop, G. Nath, Mixed convection along a vertical cone, Int. Commun. Heat Mass Tran. 16 (2) (1989) 247–255, https://doi.org/10.1016/0735-1933(89)90026-2.
[7] A.M. Abd-el Hafiz, Steady flow in an Infinite Cylindrical Pipe of a mixture Consisting of a Newtonian and a non-Newtonian phase (the case of eyring Powell model), J. Phys. Soc. Jpn. 60 (3) (1991) 879–883, https://doi.org/10.1143/JPSJ.60.879.
[8] Kafoussias Ng, MHD free convective flow through a non homogeneous porous medium over an isothermal cone surface, Mech. Res. Commun. 19 (2) (1992) 89–99, https://doi.org/10.1016/0093-6413(92)90034-8.
[9] M.A. Hossain, S.C. Paul, Free convection from a vertical permeable circular cone with non-uniform surface temperature, Acta Mech. 151 (1–2) (2001) 103–114, https://doi.org/10.1007/BF01272528.
[10] N.T.M. Eldabe, A.A. Hassan, A. Mona Aa Mohamed, Effect of couple stresses on the MHD of a non-Newtonian unsteady flow between two parallel porous plates, Z. Naturforsch. 58 (4) (2003) 204–210, https://doi.org/10.1515/zna-2003-0405.
[11] Ahmed A. Afify, The effect of radiation on free convective flow and mass transfer past a vertical isothermal cone surface with chemical reaction in the presence of a transverse magnetic field, Can. J. Phys. 82 (6) (2004) 447–458, https://doi.org/10.1139/p04-009.

[12] Peng Xu, Tahir Cagin, William A. Goddard, Assessment of phenomenological models for viscosity of liquids based on nonequilibrium atomistic simulations of copper, J. Chem. Phys. 123 (10) (2005), https://doi.org/10.1063/1.1881052.

[13] Bapuji Pullepu, E. Ekambavanan, A.J. Chamkha, Unsteady laminar natural convection from a non-isothermal vertical cone, Nonlinear Anal. Model Control 12 (4) (2007) 525–540, https://doi.org/10.15388/NA.2007.12.4.14684.

[14] J. Zueco, O. Anwar Bég, Network numerical simulation applied to pulsatile non-Newtonian flow through a channel with couple stress and wall mass flux effects, Int. J. Appl. Math. Mech. 5 (2) (2009) 1–16.

[15] Hema C. Surati, M.G. Timol, Numerical study of forced convection wedge flow of some non-Newtonian fluids, Int. J. Appl. Math. Mech. 6 (18) (2010) 50–65.

[16] Bapuji Pullepu, P. Sambath, Free convection flow of dissipative fluid from nonisothermal vertical cone, J. Eng. Phys. Thermophys. 87 (2014) 962–972, https://doi.org/10.1007/s10891-014-1094-1.

[17] M.A.A. Hamad, Analytical solution of natural convection flow of a nanofluid over a linearly stretching sheet in the presence of magnetic field, Int. Commun. Heat Mass Tran. 38 (4) (2011) 487–492, https://doi.org/10.1016/j.icheatmasstransfer.2010.12.042.

[18] Sami Ullah Khan, Nasir Ali, Zaheer Abbas, Influence of heat generation/absorption with convective heat and mass conditions in unsteady flow of eyring Powell nanofluid over porous oscillatory stretching surface, Journal of Nanofluids 5 (3) (2016) 351–362, https://doi.org/10.1166/jon.2016.1224.

[19] Imad Khan, Mair Khan, M.Y. Malik, T. Salahuddin, et al., Mixed convection flow of eyring-powell nanofluid over a cone and plate with chemical reactive species, Results Phys. 7 (2017) 3716–3722, https://doi.org/10.1016/j.rinp.2017.08.042.

[20] B. Prabhavathi, P Sudarsana Reddy, R. Bhuvana Vijaya, Chamkha Ali, et al., MHD boundary layer heat and mass transfer flow over a vertical cone embedded in porous media filled with Al2O3-water and Cu-water nanofluid, Journal of Nanofluids 6 (5) (2017) 883–891, https://doi.org/10.1166/jon.2017.1380.

[21] P Sudarsana Reddy, J Chamkha Ali, Heat and mass transfer characteristics of Al2O3- water and Ag- water nanofluid through porous media over a vertical cone with heat generation/absorption, J. Porous Media 20 (1) (2017), https://doi.org/10.1615/JPorMedia.v20.i1.10.

[22] B.V. Swarnalathamma, Heat and mass transfer on MHD flow of nanofluid with thermal slip effects, Int. J. Appl. Eng. Res. 13 (18) (2018) 13705–13726.

[23] Adesanya Samuel Olumide, Ogunseye Hammed Abiodun, Jangili Srinivas, Unsteady squeezing flow of a radiative eyring-powell fluid channel flow with chemical reactions, Int. J. Therm. Sci. 125 (2018) 440–447, https://doi.org/10.1016/j.ijthermalsci.2017.12.013.

[24] Saima Noreen, Magneto-thermo hydrodynamic peristaltic flow of eyring-powell nanofluid in asymmetric channel, Nonlinear Eng. 7 (2) (2018) 83–90, https://doi.org/10.1515/nleng-2017-0069.

[25] Khan Abdul Samad, Yufeng Nie, Zahir Shah, Abdullah Dawar, Waris Khan, Saeed Islam, Three-dimensional nanofluid flow with heat and mass transfer analysis over a linear stretching surface with convective boundary conditions, Appl. Sci. 8 (11) (2018) 2244, https://doi.org/10.3390/app8112244.

[26] P. Sambath, Bapuji Pullepu, T. Hussain, Sabir Ali Shehzad, Radiated chemical reaction impacts on natural convective MHD mass transfer flow induced by a vertical cone, Results Phys. 8 (2018) 304–315, https://doi.org/10.1016/j.rinp.2017.12.005.

[27] Kotnurkar Asha Shivappa, Sunitha Giddaiah, Bioconvection peristaltic flow of nano eyring–powell fluid containing gyrotactic microorganism, SN Appl. Sci. 1 (10) (2019) 1276, https://doi.org/10.1007/s42452-019-1281-y.

[28] K Anantha Kumar, B. Ramadevi, V. Sugunamma, JV Ramana Reddy, Heat transfer characteristics on MHD powell-eyring fluid flow across a shrinking wedge with non-uniform heat source/sink, J. Mech. Eng. Sci. 13 (1) (2019) 4558–4574, https://doi.org/10.15282/jmes.13.1.2019.15.0385.

[29] Subharthi Sarkar, Mehari Fentahun Endalew, Effects of melting process on the hydromagnetic wedge flow of a casson nanofluid in a porous medium, Bound. Value Probl. 2019 (1) (2019) 1–14, https://doi.org/10.1186/s13661-019-1157-5.

[30] T Eldabe Nabil, Raafat R. Rizkalla, Mohamed Y. Abouzeid, Vivian M. Ayad, Thermal diffusion and diffusion thermo effects of eyring-powell nanofluid flow with gyrotactic microorganisms through the boundary layer, Heat Tran. Asian Res. 49 (1) (2020) 383–405, https://doi.org/10.1002/htj.21617.

[31] Sami Ullah Khan, Waqas Hassan, Taseer Muhammad, Muhammad Im- ran, Shaban Aly, Simultaneous effects of bioconvection and velocity slip in three-dimensional flow of eyring-powell nanofluid with arrhenius activation energy and binary chemical reaction, Int. Commun. Heat Mass Tran. 117 (2020) 104738, https://doi.org/10.1016/j.icheatmasstransfer.2020.104738.

[32] Fazal Haq, Muhammad Ijaz Khan, Sohail A. Khan, T. Hayat, Investigation of suspended nanoliquid flow of eyring–powell fluid with gyrotactic microorganisms and density number, Adv. Mech. Eng. 12 (9) (2020) 1687814020924894, https://doi.org/10.1177/1687814020924894.

[33] Sami Ullah Khan, Hafiz Muhammad Ali, Swimming of gyrotactic microorganisms in unsteady flow of eyring Powell nanofluid with variable thermal features: some bio-technology applications, Int. J. Thermophys. 41 (2020) 1–19, https://doi.org/10.1007/s10765-020-02736-2.

[34] Muhammad Bilal, Samia Ashbar, Flow and heat transfer analysis of eyring-powell fluid over stratified sheet with mixed convection, Journal of the Egyptian Mathematical Society 28 (1) (2020) 1–16, https://doi.org/10.1186/s42787-020-00103-6.

[35] Kotha Gangadhar, Kolipaula Venkata Ramana, Munagala Venkata Subba Rao, Surekha Penki, J Chamkha Ali, Internal heat generation on bioconvection of an MHD nanofluid flow due to gyrotactic microorganisms, The European Physical Journal Plus 135 (2020) 1–19, https://doi.org/10.1140/epjp/s13360-020-00606-2.

[36] H.T. Basha, R. Sivaraj, Entropy generation of peristaltic eyring–powell nanofluid flow in a vertical divergent channel for biomedical applications, Proc. IME E J. Process Mech. Eng. 235 (5) (2021) 1575–1586, https://doi.org/10.1177/09544089211013926.

[37] Wei-Feng Xia, Fazal Haq, Muzher Saleem, M Ijaz Khan, Sami Ullah Khan, Yu-Ming Chu, Irreversibility analysis in natural bio-convective flow of eyring-powell nanofluid subject to activation energy and gyrotactic microorganisms, Ain Shams Eng. J. 12 (4) (2021) 4063–4074, https://doi.org/10.1016/j.asej.2021.03.016.

[38] Fazal Haq, Muzher Saleem, M Ijaz Khan, Yasser Elmasry, Chinram Ronna- son, Entropy generation minimization in bio-convective flow of nanofluid with activation energy and gyrotactic micro-organisms, AIP Adv. 11 (5) (2021), https://doi.org/10.1063/5.0047567.

[39] K. Gangadhar, J Chamkha Ali, et al., Entropy minimization on magnetized Boussinesq couple stress fluid with non-uniform heat generation, Phys. Scripta 96 (9) (2021) 095205, https://doi.org/10.1088/1402-4896/ac03de.

[40] R Edukondala Nayak Kotha Gangadhar, M. Venkata Subba Rao, T. Kannan, Nodal/saddle stagnation point slip flow of an aqueous convectional magnesium oxide–gold hybrid nanofluid with viscous dissipation, Arabian J. Sci. Eng. 46 (2021) 2701–2710, https://doi.org/10.1007/s13369-020-05195-x.

[41] Prashanta Kumar Mandal, Seth Gauri Shanker, Subharthi Sarkar, Chamkha Ali, A numerical simulation of mixed convective and arbitrarily oblique radiative stagnation point slip flow of a CNT-water MHD nanofluid, J. Therm. Anal. Calorim. 143 (2021) 1901–1916, https://doi.org/10.1007/s10973-020-10344-3.

[42] M Ijaz Khan, Faisal Shah, Sami Ullah Khan, Abuzar Ghaffari, Yu- Ming Chu, et al., Heat and mass transfer analysis for bioconvective flow of eyring Powell nanofluid over a riga surface with nonlinear thermal features, Numer. Methods Part. Differ. Equ. 4 (2022) 777–793, https://doi.org/10.1002/num.22696.

[43] Bharatkumar Manvi, Jagadish Tawade, Mahadev Biradar, Samad Noeiaghdam, Unai Fernandez-Gamiz, Vediyappan Govindan, The effects of MHD radiating and non-uniform heat source/sink with heating on the momentum and heat transfer of eyring-powell fluid over a stretching, Results in Engineering 14 (2022) 100435, https://doi.org/10.1016/j.rineng.2022.100435.

[44] Salman Saleem, Degavath Gopal, Nehad Ali Shah, Nosheen Feroz, Naikoti Kishan, Jae Dong Chung, Saleha Safdar, Modelling entropy in magnetized flow of eyring–powell nanofluid through nonlinear stretching surface with chemical reaction: a finite element method approach, Nanomaterials 12 (11) (2022) 1811, https://doi.org/10.3390/nano12111811.

[45] Sadique Rehman, Aisha Anjum, M. Farooq, M.Y. Malik, et al., Melting heat phenomenon in thermally stratified fluid reservoirs (Powell-Eyring fluid) with Joule heating, Int. Commun. Heat Mass Tran. 137 (2022) 106196, https://doi.org/10.1016/j.icheatmasstransfer.2022.106196.

[46] K Thanesh Kumar Jyoti Atul Dhanke, Pudhari Srilatha, Kurapati Swarnalatha, P. Satish, S. Abdul Gaffar, Magnetohydrodynamic radiative simulations of eyring–powell micropolar fluid from an isothermal cone, Int. J. Algorithm. Comput. Math. 8 (5) (2022) 232, https://doi.org/10.1007/s40819-022-01436-9.

[47] Surya Kanta Mondal, Dulal Pal, Entropy optimization and heat transfer analysis of magneto-bioconvective Powell eyring nanofluid with nonlinear thermal radiation and chemical reaction over a stretching sheet, Journal of Nanofluids 11 (6) (2022) 996–1008, https://doi.org/10.1166/jon.2022.1886.

[48] S. Arulmozhi, K. Sukkiramathi, S.S. Santra, R. Edwan, Unai Fernandez-Gamiz, Samad Noeiaghdam, Heat and mass transfer analysis of radiative and chemical reactive effects on MHD nanofluid over an infinite moving vertical plate, Results in Engineering 14 (2022) 100394, https://doi.org/10.1016/j.rineng.2022.100394.

[49] G. Dharmaiah, S. Dinarvand, P. Durgaprasad, S. Noeiaghdam, Arrhenius activation energy of tangent hyperbolic nanofluid over a cone with radiation absorption, Results in Engineering 16 (2022) 100745, https://doi.org/10.1016/j.rineng.2022.100745.

[50] R Ali Shah Aamir Saeed, M Sohail Khan, Unai Fernandez-Gamiz, Z Bani-Fwaz Mutasem, Samad Noeiaghdam, M Galal Ahmed, Theoretical analysis of unsteady squeezing nanofluid flow with physical properties, Math. Biosci. Eng. 19 (10) (2022) 10176–10191.

[51] Jagadish V. Tawade, C.N. Guled, Samad Noeiaghdam, Unai Fernandez- Gamiz, Vediyappan govindan, and sundarappan balamuralitharan, effects of thermophoresis and brownian motion for thermal and chemically reacting casson nanofluid flow over a linearly stretching sheet, Results in Engineering 15 (2022) 100448, https://doi.org/10.1016/j.rineng.2022.100448.

[52] Kotha Gangadhar, Manda Aruna Kumari, J Chamkha Ali, EMHD flow of radiative second-grade nanofluid over a riga plate due to convective heating: revised buongiorno's nanofluid model, Arabian J. Sci. Eng. 47 (7) (2022) 8093–8103, https://doi.org/10.1007/s13369-021-06092-7.

[53] Susmay Nandi, Bidyasagar Kumbhakar, Subharthi Sarkar, MHD stagnation point flow of Fe3O4/Cu/Ag-CH3OH nanofluid along a convectively heated stretching sheet with partial slip and activation energy: numerical and statistical approach, Int. Commun. Heat Mass Tran. 130 (2022) 105791, https://doi.org/10.1016/j.icheatmasstransfer.2021.105791.

[54] P.K. Mandal, A.K. Singha, B. Kumar, G.S. Seth, S. Sarkar, Analysis of unsteady magnetohydrodynamic 3-D rotating flow and transfer of heat in carbon nanotube-water nanofluid: an engineering application, Journal of Nanofluids 11 (2) (2022) 204–213, https://doi.org/10.1166/jon.2022.1826.

[55] Muhammad Sohail Khan, Mei Sun, Unai Fernandez-Gamiz Shabnam, Samad Noeiaghdam, Aamir Khan, Numerical simulation of a time-dependent electroviscous and hybrid nanofluid with Darcy-forchheimer effect between squeezing plates, Nanomaterials 12 (5) (2022) 876, https://doi.org/10.3390/nano12050876.

[56] Kotha Gangadhar, E. Mary Victoria, J Chamkha Ali, Hydrothermal Features in the Swirling Flow of Radiated Graphene–Fe3O4 Hybrid Nanofluids through a Rotating Cylinder with Exponential Space-dependent Heat Generation, Waves in Random and Complex Media, 2022, pp. 1–24, https://doi.org/10.1080/17455030.2022.2100004.

[57] Dhanekula Naga Bhargavi, Kotha Gangadhar, J Chamkha Ali, Graphene-Gold/PDMS maxwell hybrid nanofluidic flow in a squeezed channel with linear and irregular radiations, Proc. IME E J. Process Mech. Eng. (2022) 09544089221139696, https://doi.org/10.1177/09544089221139696.

[58] K. Gangadhar, P. Manasa Seshakumari, M. Venkata Subba Rao, J Chamkha Ali, Bioconvective transport of magnetized couple stress fluid over a radiative paraboloid of revolution, Proc. IME E J. Process Mech. Eng. 236 (4) (2022) 1661–1670, https://doi.org/10.1177/09544089211072715.

[59] K. Gangadhar, K. Bhanu Lakshmi, T. Kannan, J Chamkha Ali, Bioconvective Magnetized Oldroyd-B Nanofluid Flow in the Presence of Joule Heating with Gyrotactic Microorganisms, Waves in Random and Complex Media, 2022, pp. 1–21, https://doi.org/10.1080/17455030.2022.2050441.

[60] K Bhanu Lakshmi Kotha Gangadhar, Shreen El-Sapa, M. Venkata Subba Rao, J Chamkha Ali, Thermal Energy Transport of Radioactive Nanofluid Flow Submerged with Microorganisms with Zero Mass Flux Condition, Waves in Random and Complex Media, 2022, pp. 1–23, https://doi.org/10.1080/17455030.2022.2072536.

[61] Kotha Gangadhar, Manda Aruna Kumari, M. Venkata Subba Rao, J Chamkha Ali, Oldroyd-B nanoliquid flow through a triple stratified medium submerged with gyrotactic bioconvection and nonlinear radiations, Arabian J. Sci. Eng. (2022) 1–13, https://doi.org/10.1007/s13369-021-06412-x.

[62] G. Dharmaiah, JL Rama Prasad, K.S. Balamurugan, I. Nurhidayat, Unai Fernandez-Gamiz, Samad Noeiaghdam, Performance of magnetic dipole contribution on ferromagnetic non-Newtonian radiative MHD blood flow: an application of biotechnology and medical sciences, Heliyon 9 (2) (2023), https://doi.org/10.1016/j.heliyon.2023.e13369.

[63] Kotha Gangadhar, R Edukondala Nayak, M. Venkata Subba Rao, J Chamkha Ali, Nonlinear radiations in chemically reactive walter's B nanoliquid flow through a rotating cone, Proc. IME E J. Process Mech. Eng. 237 (3) (2023) 731–739, https://doi.org/10.1177/09544089221105932.

[64] Kotha Gangadhar, M. Prameela, J Chamkha Ali, Exponential space-dependent heat generation on powell–eyring hybrid nanoliquid under nonlinear thermal radiation, Indian J. Phys. (2023) 1–13, https://doi.org/10.1007/s12648-022-02585-9.

[65] Mehari Fentahun Endalew, Subharthi Sarkar, et al., Modeling and analysis of unsteady casson fluid flow due to an exponentially accelerating plate with thermal and solutal convective boundary conditions, J. Appl. Math. (2023) 2023, https://doi.org/10.1155/2023/3065357.

[66] Mehari Fentahun Endalew, Subharthi Sarkar, Numerical exploration of forced convection hydromagnetic hyperbolic tangent nanofluid flow over a permeable wedge with melting heat transfer, Sci. Rep. 13 (1) (2023) 3515, https://doi.org/10.1038/s41598-023-30656-2.

[67] P. Patil, B. Goudar, Impact of impulsive motion on the eyring-powell nanofluid motion across a rotating sphere in MHD convective regime: entropy analysis, J. Magn. Magn Mater. 571 (2023) 170590, https://doi.org/10.1016/j.jmmm.2023.170590.

[68] P. Patil, B. Goudar, E. Momoniat, Magnetized bioconvective micropolar nanofluid flow over a wedge in the presence of oxytactic microorganisms, Case Stud. Therm. Eng. 49 (2023) 103284, https://doi.org/10.1016/j.csite.2023.103284.

[69] P. Patil, A. Shashikant, E. Momoniat, Analysis of sodium chloride and sucrose diffusions in mixed convective nanoliquid flow, Ain Shams Eng. J. 12 (2) (2021) 2117–2124, https://doi.org/10.1016/j.asej.2020.10.008.

[70] P.M. Patil, S.H. Doddagoudar, P.S. Hiremath, E. Momoniat, Influence of applied magnetic field on mixed convective nanofluid flow past an exponentially stretching surface with roughness, J. Braz. Soc. Mech. Sci. Eng. 41 (2019) 1–11, https://doi.org/10.1007/s40430-019-2065-4.

[71] P.M. Patil, M. Kulkarni, J.R. Tonannavar, A computational study of the triple-diffusive nonlinear convective nanoliquid flow over a wedge under convective boundary constraints, Int. Commun. Heat Mass Tran. 128 (2021) 105561, https://doi.org/10.1016/j.icheatmasstransfer.2021.105561.

[72] P.M. Patil, N. Kumarwadi, Effects of MHD mixed convection with non-uniform heat source/sink and cross-diffusion over exponentially stretching sheet, Int. J. Numer. Methods Heat Fluid Flow 28 (6) (2018) 1238–1255, https://doi.org/10.1108/HFF-04-2017-0149.

[73] P.M. Patil, E. Momoniat, S. Roy, Influence of convective boundary condition on double diffusive mixed convection from a permeable vertical surface, Int. J. Heat Mass Tran. 70 (2014) 313–321, https://doi.org/10.1016/j.ijheatmasstransfer.2013.11.021.

[74] P.M. Patil, H.F. Shankar, Heat transfer attributes of Al2O3-Fe3O4/H2O hybrid nanofluid flow over a yawed cylinder, Propulsion and Power Research 11 (3) (2022) 416–429, https://doi.org/10.1016/j.jppr.2022.06.002.

[75] P.M. Patil, H.F. Shankar, Analysis of nonlinear thermal radiation and entropy on combined convective ternary (SWCNT-MWCNT-Fe3O4) eyring–powell nanoliquid flow over a slender cylinder, Numer. Heat Tran., Part A: Applications (2023) 1–21, https://doi.org/10.1080/10407782.2023.2195131.

[76] P.M. Patil, A. Shashikant, Unsteady mixed convection along a permeable exponentially stretching surface: influence of velocity slip and thermal jump, Int. J. Numer. Methods Heat Fluid Flow 28 (9) (2018) 1994–2011, https://doi.org/10.1108/HFF-07-2017-0283.